Journal of
*Marine Science and Engineering*

MDPI

*Article*

# Revisiting the Upwelling Evolution along the Western Iberian Peninsula over the 21st Century Using Dynamically Downscaled CMIP6 Data

**Brieuc Thomas *, Xurxo Costoya, Maite deCastro and Moncho Gómez-Gesteira**

Environmental Physics Laboratory (EPhysLab), Centro de Investigación Mariña, Universidade de Vigo, Campus da Auga, 32004 Ourense, Spain; xurxocostoya@uvigo.gal (X.C.); mdecastro@uvigo.es (M.d.); mggesteira@uvigo.es (M.G.-G.)
* Correspondence: brieuc.thomas@uvigo.gal

**Abstract:** Coastal upwelling is of particular importance in the western Iberian Peninsula, considering its socioeconomic impact on the region. Therefore, it is of crucial interest to evaluate how climate change, by modifying wind patterns, might influence its intensity and seasonality. Given the limited spatial extension of the area, it is essential to use high-resolution data. Thus, the weather research and forecasting model was used to dynamically downscale data from a multi-model ensemble from the 6th phase of the Coupled Model Intercomparison Project, representing the latest climate projections. Two shared socioeconomic pathways, 2–4.5 and 5–8.5 scenarios, were considered. The results show that climate change will not modify the upwelling seasonality in the area, where the months from April to September represent the period of highest intensity. Conversely, this seasonality might be exacerbated throughout the 21st century, as upwelling is expected to strengthen during these months and decrease during others. Additionally, coastal upwelling shows the highest increase at the northerner locations of the western Iberian Peninsula, resulting in a homogenization of its intensity along this coast. These changes may result from the anticipated intensification and northward shift of the Azores High.

**Keywords:** coastal upwelling; western Iberian Peninsula; Azores high; CMIP6 projections; WRF dynamical downscaling



**Citation:** Thomas, B.; Costoya, X.; deCastro, M.; Gómez-Gesteira, M. Revisiting the Upwelling Evolution along the Western Iberian Peninsula over the 21st Century Using Dynamically Downscaled CMIP6 Data. *J. Mar. Sci. Eng.* **2024**, *12*, 1494. https://doi.org/10.3390/jmse12091494

Academic Editor: Eugen Rusu

Received: 26 July 2024
Revised: 25 August 2024
Accepted: 26 August 2024
Published: 29 August 2024



## 1. Introduction

Coastal upwelling plays a crucial economic role, accounting for about 20% of global wild marine capture fisheries, even though the regions where it occurs cover only approximately 2% of the world's ocean surface [1]. Indeed, the upwelling of cold, nutrient-rich waters stimulates biological activity along the coast. The Canary Upwelling Ecosystem (CUE), stretching from 12° N to 43° N, is one of the world's four major eastern boundary upwelling systems. The CUE is divided into various sub-regions based on their unique physical environments, shelf dynamics, and circulation patterns. One of them, the western Iberian Peninsula (WIP), encompassing the west coasts of Galicia and Portugal (37–43° N), experiences seasonal upwelling driven by the seasonal shifts in the zonal wind component, which are influenced by the position of the Azores High. Basically, northerly winds, which blow parallel to the coast, prevail during summer on the western coast of the Iberian Peninsula. Due to the Coriolis effect, surface water is deflected westward away from the coast. This movement of surface water creates a partial vacuum near the coast, which is filled by colder, nutrient-rich waters rising from deeper ocean layers [2–4].

Coastal upwelling systems have been extensively studied, particularly regarding their spatial and temporal variability. Bakun (1990) [5] proposed that global warming might intensify alongshore wind stress, thereby enhancing coastal upwelling. Since then, numerous studies have explored this hypothesis across different upwelling regions, utilizing

historical wind data, and have endeavored to uncover how upwelling systems respond to climate change, their findings being inconsistent [6–10]. Some of them have indicated a weakening in upwelling intensity, which contradicts Bakun's hypothesis and reveals a high dependence on the region, season, data length, and database used. Actually, Sydeman et al. (2014) [11] reviewed multiple studies that showed different results, emphasizing these dependencies. About the CUE, Varela et al. (2015) [12] found an increasing trend in upwelling between 1982 and 2010.

Considering the socioeconomic importance of coastal upwelling systems, it is essential to understand how climate change may affect wind patterns and, therefore, the intensity and seasonality of upwelling phenomena. Climate models are crucial tools for this purpose, offering robust projections. The latest compilation of general circulation models (GCMs), presented in the 6th phase of the Coupled Model Intercomparison Project (CMIP6) [13], provides comprehensive climate projections based on various future greenhouse gas (GHG) emission scenarios known as shared socioeconomic pathways (SSPs) [14]. These scenarios account for different assumptions about population growth, education, urbanization, and gross domestic product (GDP) to estimate future GHG emissions. The previous CMIP version (CMIP5) used climate scenarios known as representative concentration pathways (RCPs), solely based on GHG emissions projections [15].

However, GCMs have a relatively coarse resolution since they model the entire Earth's atmosphere and oceans, which limits their ability to analyze regional climate impacts in detail. To address this, dynamical downscaling using regional climate models (RCMs) is employed. RCMs, when forced with GCM data, offer a much finer spatial resolution and can incorporate specific regional characteristics, making them more suitable for localized studies. It is also important to validate the reliability of these climate models in accurately replicating wind patterns for specific regions. This validation involves comparing historical model simulations with observational data. Models that show strong statistical alignment with observed data are considered reliable for future projections, making them valuable for assessing changes in wind patterns due to climate change.

Several studies explored the changes in coastal upwelling, induced by modified wind patterns under future greenhouse warming, in the major eastern boundary upwelling systems using CMIP5 data [16,17]. Along the Iberian Peninsula, representing the northern part of the CUE, this topic has been investigated using regional climate projections from CORDEX (Coordinated Regional Climate Downscaling Experiment) data, based on CMIP5. Alvarez et al. (2016) [18] examined trends in upwelling intensity along the Galician coast and predicted a strengthening in upwelling intensity from April to September. According to Sousa et al. (2017) [19], global warming will significantly impact upwelling intensity along the WIP throughout the 21st century. They suggest a general increase in upwelling strength for nearly all latitudes, with the most pronounced intensification expected in the northern regions, particularly above 41.5° N, caused by an intensification and a displacement northward of the Azores High. Several studies highlighted the influence of the Azores High's position and intensity on the CUE, both in its southern [20] and northern [21] sections, also using CMIP5 data. Nevertheless, no study analyzing the changes in coastal upwelling using CMIP6 dynamically downscaled wind data has been performed yet, neither for the CUE nor for the other eastern boundary upwelling systems.

This work aims to assess the evolution of the upwelling intensity and seasonality in the WIP (see Figure 1) throughout the 21st century using dynamical downscaling of a CMIP6 multi-model ensemble. Given the limited spatial extent of the study area, high-resolution spatial data was used through the weather research and forecasting (WRF) model. This research examines both the historical and future climatology of upwelling, as well as the trends representing its evolution over the 21st century. Future scenarios SSP2–4.5 and SSP5–8.5, representing intermediate and high greenhouse gas emissions, respectively, were considered. Additionally, the study analyzed the evolution of the position and intensity of the Azores High.

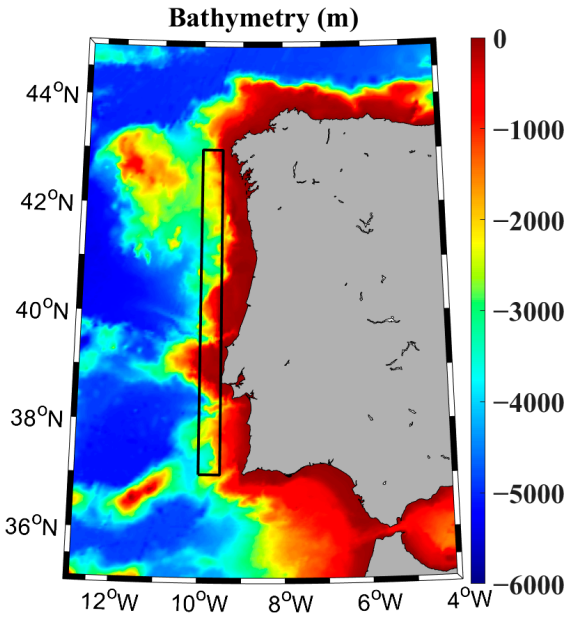


**Figure 1.** Bathymetry (m) of the area under study. Black rectangle marks the area where coastal upwelling evolution is analyzed.

## 2. Data and Methods

### *2.1. WRF Dynamical Downscaling*

Considering that coastal upwelling is a process that needs to be analyzed at a regional scale, high-resolution wind data are necessary. Therefore, wind speed and direction at 10 m height were determined through a dynamic downscaling method employing the WRF-ARW v4.3.3 meteorological model [22]. Initial and boundary conditions were supplied by Xu et al. (2021) [23] at a spatial resolution of 1.25° and a temporal resolution of 6 h. This dataset spans from 1985 to 2014 historically and from 2015 to 2100 into the future based on SSP2–4.5 and SSP5–8.5 scenarios. It incorporates an ensemble of 18 GCMs from the CMIP6 project to account for long-term trends, alongside the internal climate variability from a single CMIP6 model (MPI-ESM1-HR). Furthermore, this dataset underwent bias correction using information from the ERA5 reanalysis [24] from 1979 to 2014. Xu et al. (2021) [23] detailed a process involving the decomposition of CMIP6 GCM data (MPI-ESM1-HR) into long-term and short-term components, with subsequent bias corrections to enhance accuracy.

The WRF setup involved two simulation domains. The main domain, labeled D01 in Figure 2, has a spatial resolution of 30 km, whereas the nested domain D02 uses a spatial resolution of 10 km. This configuration facilitated the generation of future wind datasets with the required spatial detail for in-depth analyses along the WIP coastline, as well as sea level pressure (SLP) data in the Atlantic Ocean zone where the Azores High operates.

Simulations were conducted for a historical period (1985–2014) and a future one (2020–2100) under the SSP2–4.5 and SSP5–8.5 scenarios. To ensure the accuracy of the WRF model and avoid error accumulation, simulations were executed daily with a 12 h spin-up period. Each run covers a period of 36 h, commencing at 12:00 UTC on the preceding day of interest. This approach, as utilized in prior WRF downscaling studies [25–30], enhances precision and can help reduce the computational cost compared to continuous simulations across the entire period, as the daily simulations can be run in parallel. Additionally, specific parameterizations were utilized, including the Thompson microphysics scheme [31], the Yonsei University planetary boundary layer scheme [32], the United Noah land surface model [33], the Revised MM5 surface layer scheme [34], the RRTMG shortwave and longwave radiation schemes [35], and the New Tiedtke cumulus parameterization [36].

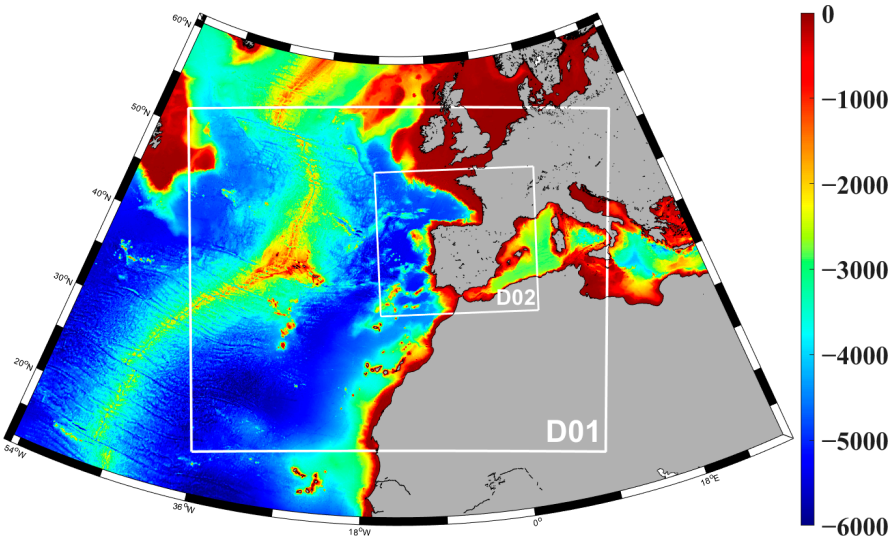


**Figure 2.** Bathymetry (m) of the study area and the simulation domains (indicated by white lines) used in WRF.

These same input data and parametrizations were used by Thomas et al. (2023) [30] with highly similar domains, and they performed a validation of the modeled wind data that showed great results in the area under study. The output provided data with a 6 h temporal resolution. In the WIP, where the upwelling is studied, 10 m height wind data present a 10 km spatial resolution, while SLP data are obtained with a 30 km resolution in the area covering the Azores High.

### *2.2. Computation and Validation of the Data*

#### 2.2.1. Calculation of the Upwelling Index

In the study area, extending from −10° to −9.5° longitude and 37° to 43° latitude (black rectangle in Figure 1), the Ekman transport was calculated for each grid point from the WRF simulations based on the zonal and meridional wind speeds, respectively, $W_x$ and $W_y$:

$$Q_x = \frac{\rho_a C_d}{\rho_w f} \sqrt{{W_x}^2 + {W_y}^2} W_y \quad (1)$$

$$Q_y = -\frac{\rho_a C_d}{\rho_w f} \sqrt{{W_x}^2 + {W_y}^2} W_x \quad (2)$$

where $\rho_a = 1.225\ kgm^{-3}$ is the air density, $C_d = 1.4 \times 10^{-3}$ is a dimensionless drag coefficient, $\rho_w = 1025\ kgm^{-3}$ is the sea water density, and $f = 2\Omega\sin(\theta)$ is the Coriolis parameter, $\Omega$ being the vertical component of the Earth's angular velocity and $\theta$ the latitude [18]. According to Equations (1) and (2), $Q_x$ and $Q_y$ are given in $m^2s^{-1}$. Then, the upwelling index (UI), which is basically the Ekman transport in the direction perpendicular to the shoreline, is calculated by means of the next formula:

$$UI = -Q_x \sin\left(\varphi - \frac{\pi}{2}\right) + Q_y \cos\left(\varphi - \frac{\pi}{2}\right) \quad (3)$$

where $\varphi$ is the angle defined by a unitary vector perpendicular to the shoreline and pointing seaward [18]. Despite slight variations in the shoreline angle along its coast, the WIP shoreline maintains an angle close to 90° relative to the equator. Therefore, the value of $\varphi$ is approximated to $\pi$ and the UI in this area is defined by $UI = -Q_x$. Positive values represent upwelling favorable conditions, and vice-versa. It should be noted that the values of UI shown in this study are multiplied by 1000 in order to be expressed in $m^3s^{-1}km^{-1}$, representing the flow of water moved through one kilometer of coast. UI values were obtained with a daily temporal resolution.

#### 2.2.2. Validation of the Results

The accuracy of simulated UI values in WIP was assessed by comparison with ERA5 data [24] by means of the overlapping percentage function (OP, [30,37]). The OP is used to measure the degree of similarity or overlap between two sets (Equation (4)). ERA5 zonal and meridional wind data at 10 m above sea level were used to calculate UI values with a spatial resolution of 0.25° and an hourly temporal resolution for the 1985–2014 period, corresponding to the WRF historical period. Given the different spatial resolutions between the WRF (10 km) and ERA5 (0.25°) datasets, a linear interpolation of the higher-resolution WRF grid to match the ERA5 one was performed specifically for this validation. Additionally, because the datasets have different temporal resolutions, daily mean values were computed for both. Then, the probability density function of each UI series was calculated for each grid point (Figure 1) using bins of 50 $m^3s^{-1}km^{-1}$, ranging from −2000 to 2000 $m^3s^{-1}km^{-1}$, for both datasets. Lastly, the OP is calculated using the following formula:

$$OP(\%) = 100 \times \sum_{i=1}^{n} \text{minimum}\left(Z_i^{WRF}, Z_i^{ERA5}\right) \quad (4)$$

where n represents the number of bins and $Z_i$ is the frequency of occurrence of the corresponding UI range from the WRF or ERA5 dataset. This metric calculates the cumulative minimum value of two distributions of each binned value, thereby measuring the common area between two probability density functions.

### *2.3. Spatiotemporal Evolution of the Upwelling Index*

In order to estimate the future evolution of the UI in the study area, a complete analysis with different steps was carried out. First, its climatology was computed. The data were separated into three 30-year periods: historical (1985–2014), near future (2030–2059), and far future (2070–2099), both future periods under SSP2–4.5 and SSP5–8.5. Moreover, the data, ranging from 37° N to 43° N in latitude, were separated into six intervals covering 1° in latitude. Then, for each of these groups (defined by their period and coverage area), the average value and standard deviation of UI were calculated for each month of the climatic year, meaning monthly values are obtained considering the 30 years of the period.

After that, monthly trends were computed. For this purpose, the entire future period (2020–2100, under both SSPs) was considered, and by dividing the data into 0.25° latitude intervals (from 37° N to 43° N), the average UI values of each month were also computed. Thus, monthly climatic values were obtained, in the same way as described above. Then, UI trends were computed by performing a linear regression on the data, for each month and each latitude range.

Lastly, considering the same ranges of latitude but only the months of clear upwelling situation (meaning positive UI values), the differences in UI between the far future (2070–2099) and historical (1985–2014) periods were computed and represented by the ΔUI (%) variable. This analysis permits us to evaluate how the upwelling intensity will evolve in the future, for the months when it is already considered the most intense nowadays.

### *2.4. Spatiotemporal Evolution of the Azores High*

Winds in the WIP are greatly influenced by the position of the Azores High, a large, stable high-pressure system that forms over the subtropical region of the eastern North Atlantic Ocean. Therefore, its evolution throughout the 21st century has been analyzed, considering the summer months of upwelling. Sea-level pressure (SLP) data from D01 (see Figure 2) with a 30 km spatial resolution were used. SLP values were averaged at each grid point to obtain one value for every year between 2020 and 2100. Then, the 99th percentile highest SLP values and corresponding locations were obtained, considering all the grid points from the D01 domain located in the Atlantic waters. Linear interpolations of the yearly data of maximum SLP, as well as corresponding latitude and longitude, were

performed to observe their trends throughout the 21st century. The accuracy of these trends is evaluated through the *p*-value of the Pearson correlation [38].

## 3. Results and Discussion

### *3.1. Validation of the Results*

The accuracy of the data utilized in this study was verified by comparison between WRF model outputs and ERA5 reanalysis data spanning from 1985 to 2014. The agreement between these datasets was assessed using the overlapping percentage (OP), calculated using formula 4. The results, depicted in Figure 3, demonstrate OP values ranging from 90% to 95% within the studied area (10–9.5° W and 37–43° N). Thomas et al. (2023) [30], which used the same data and methodology, found similar OP values when validating wind speed in the waters of the WIP. Therefore, this validation reinforces the reliability of the WRF model's wind simulation and the associated computation method. Near the coast, models tend to exhibit greater inaccuracies, primarily due to thermal gradients from land–sea temperature variations, the abrupt change in surface roughness between land and ocean, and the influence of local topography, which significantly affects coastal wind patterns [39]. Nevertheless, the OP coastal values shown in Figure 3, remaining higher than 80%, depict good accuracy of the modeled data.

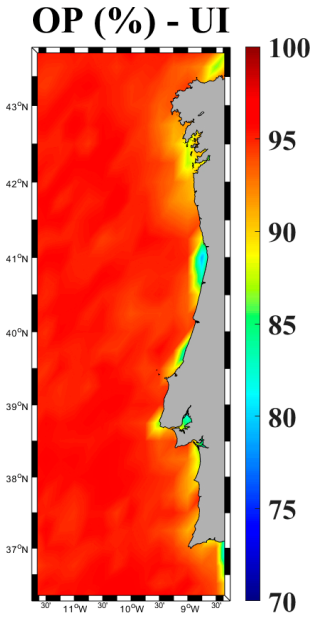


**Figure 3.** OP (%) between UI values from WRF simulation and ERA5 dataset for the 1985–2014 period.

### *3.2. Spatiotemporal Evolution of Coastal Upwelling*

#### 3.2.1. Past and Future Climatology

The UI average has been computed for areas covering 1° in latitude, from 37° N to 43° N, for every month of the climatic year. Three 30-year periods were considered to compute the climatic year: historical (1985–2014), near future (2030–2059), and far future (2070–2099), under climate scenarios SSP2–4.5 and SSP5–8.5 (Figure 4). Months from April to September correspond to clear upwelling situations, with positive UI values higher than 500 $m^3s^{-1}km^{-1}$ in all areas and for all periods. For these months, the UI is expected to vary a little in the future under SSP2–4.5 (Figure 4, left column), while the upwelling will strengthen more under SSP5–8.5 (Figure 4, right column), especially above 40° N in the far future (Figure 4b,d,f). Additionally, the months of June, July, and August show the highest values, generally over 1000 $m^3s^{-1}km^{-1}$. For the months from October to March, the UI values are quite weak and do not represent favorable conditions for upwelling. They might even be negative above 39° N in December and January, corresponding to downwelling

conditions. Future monthly UI values for the near and far futures, under SSP2–4.5 and SSP5–8.5, considering 0.25° latitude intervals, can be observed in Tables A1–A4 from Appendix A.

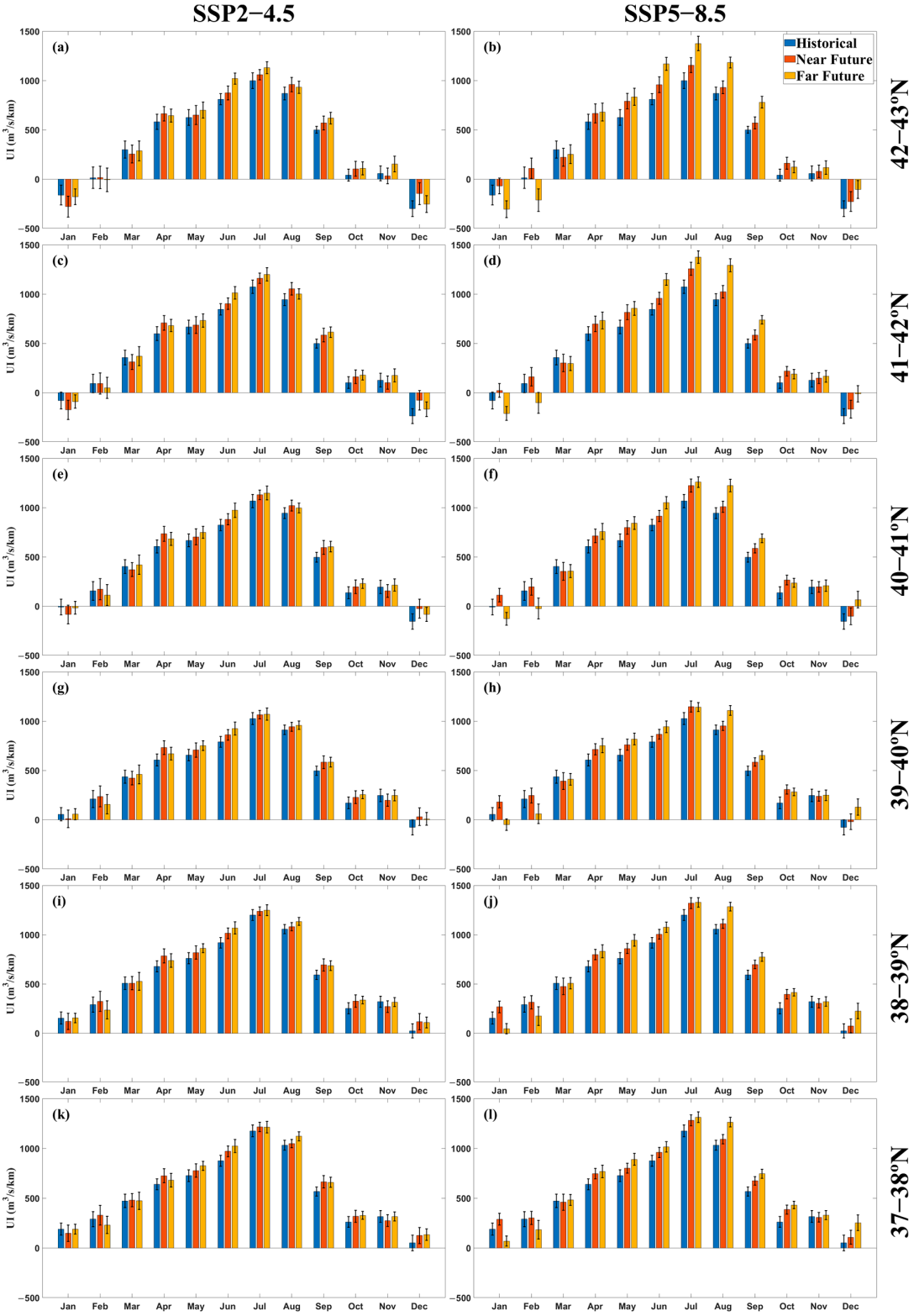


**Figure 4.** UI for the climatic year considering the historical (1985–2014), near future (2030–2059), and far future (2070–2099) periods, under SSP2–4.5 (**left column**) and SSP5–8.5 (**right column**) and for 1°-latitude intervals ranging from 37° N (**bottom** row) to 43° N (**top** row).

Picado et al. (2015) [40] obtained similar monthly UI values along the western Galician coast (42–43° N) for the period 1982–2010 using wind data from NCEP CFSR with a 0.3° spatial resolution. They observed UI values around $-200$ $m^3s^{-1}km^{-1}$ in December and January and noted a similar trend in the monthly UI distribution, with the highest values occurring between June and September. However, their summer values for the historical period do not exceed 600 $m^3s^{-1}km^{-1}$, whereas they reach 1000 $m^3s^{-1}km^{-1}$ in the present analysis. Additionally, Sousa et al. (2017) [19] found a similar UI spatial distribution along the WIP coast, with the highest UI values at latitudes around 38–39° N and slight decreases southward and northward. They used CORDEX data with a 12.5 km spatial resolution for the 1982–2005 period. Depending on the chosen CORDEX RCM data, theirs showed similar or moderately lower values than those presented in this study.

#### 3.2.2. Future Averages and Trends

Monthly UI values have been computed at 0.25° latitude intervals for the entire future period (2020–2100) under SSP2–4.5 (Figure 5a) and SSP5–8.5 (Figure 5b) scenarios. The months from April to September exhibit the highest UI values, especially July and August (~1200 $m^3s^{-1}km^{-1}$), for both climate scenarios. The UI gradually decreases for the winter months, being always under 400 $m^3s^{-1}km^{-1}$, and negative values are observed in January and December above 40° N.

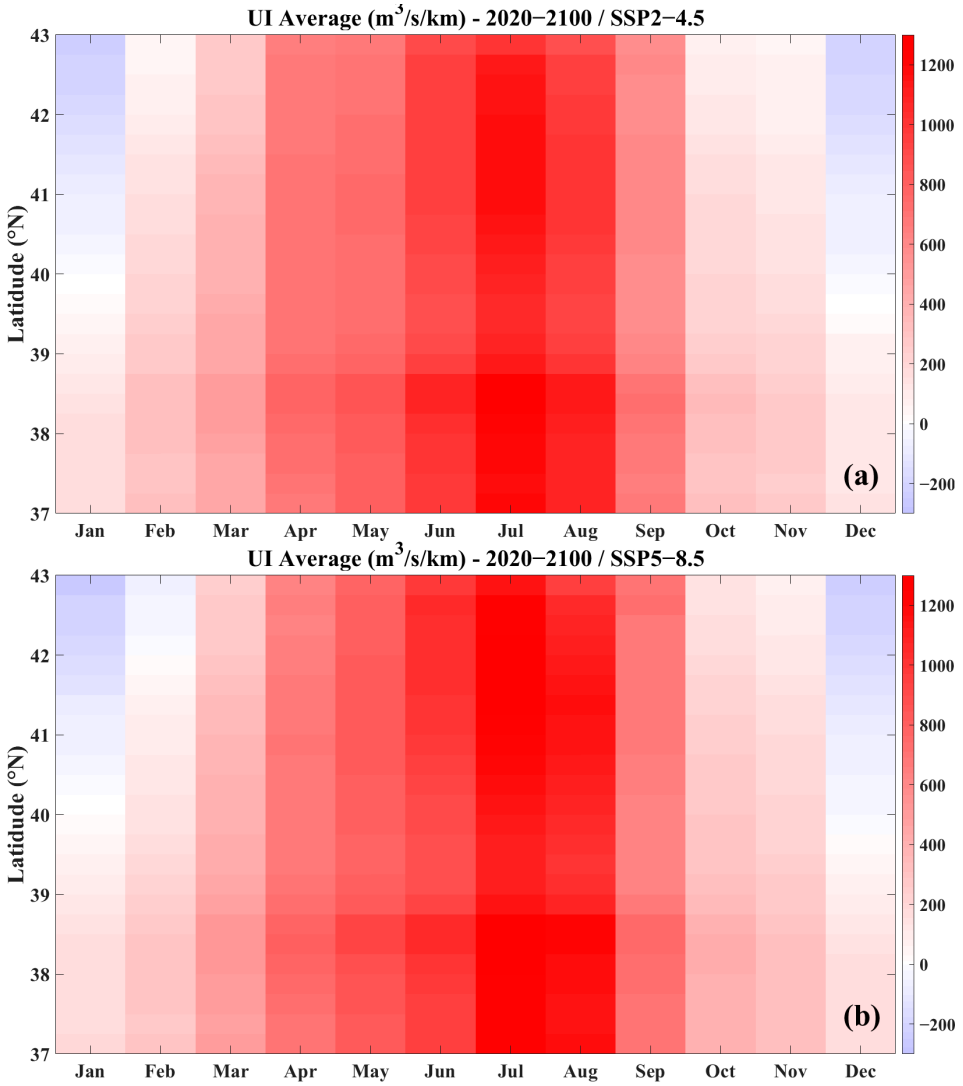


**Figure 5.** Monthly UI values at 0.25° latitude intervals for the entire future period (2020–2100) under (**a**) SSP2–4.5 and (**b**) SSP5–8.5 scenarios.

Monthly UI trends at 0.25° latitude intervals from 2020 to 2100 were obtained under SSP2–4.5 (Figure 6a) and SSP5–8.5 (Figure 6b) scenarios. Globally, both climate scenarios predict an increase in UI throughout the 21st century between May and November. Especially, upwelling intensity is expected to increase around 6 $m^3s^{-1}km^{-1}year^{-1}$ above 41° N, in June under SSP2–4.5 (Figure 6a) and between June and August under SSP5–8.5 (Figure 6b). The first climate scenario predicts a slight increase in UI (~3 $m^3s^{-1}km^{-1}year^{-1}$) in January and March for all latitudes, as well as in April above 42° N. Conversely, a decrease of around −2 $m^3s^{-1}km^{-1}year^{-1}$ is expected downward this latitude for this month, as well as in February and December at all locations (around −3 $m^3s^{-1}km^{-1}year^{-1}$). Considering SSP5–8.5, the results are quite different for these winter months. Indeed, it predicts a clear decrease in January and February, whose intensity oscillates between −2 and −4 $m^3s^{-1}km^{-1}year^{-1}$, with the highest decline found above 42° N in February. In March, no evolution of the UI is expected, while it should increase around 2 $m^3s^{-1}km^{-1}year^{-1}$ in April and 4 $m^3s^{-1}km^{-1}year^{-1}$ in December. Globally, for the summer months of historical high UI values (see Figure 4)—April to September—the UI will remain high in the future, whatever the climate scenario considered (see Figure 5) and is even expected to increase towards the end of the century with global warming (see Figure 6). On the other hand, the UI is expected to decrease for winter months, where the historical UI is insignificant or negative. Therefore, the future seasonality of the upwelling phenomenon should not be impacted by climate change, though it might be exacerbated.

In previous research, deCastro et al. (2014) [41] computed a decreasing UI trend of 8 $m^3s^{-1}km^{-1}year^{-1}$ at 37° N and insignificant values around 43° N for the months between June and August during the 1982–2012 period using NCEP CFSR wind data with a 0.5° spatial resolution. The trends computed in the present study show the opposite latitudinal pattern in the future (see Figure 6). Indeed, considering the 2020–2100 period and these same three months, the UI trend values are higher northward, reaching 2.5 and 5.5 $m^3s^{-1}km^{-1}year^{-1}$ under SSP2–4.5 and SSP5–8.5, respectively, whereas around 37° N trends are 1 and 2.5 $m^3s^{-1}km^{-1}year^{-1}$. Therefore, it appears that the intensity of the UI increase is weakening in the southern IP while strengthening northward when comparing historical and future trends. Additionally, Alvarez et al. (2016) [18] obtained trends in summer (April to September) upwelling intensity of around 0.5 $m^3s^{-1}km^{-1}year^{-1}$ in western Galicia (42–43° N, northern WIP) for the 2006–2099 period under RCP4.5 and 1 $m^3s^{-1}km^{-1}year^{-1}$ under RCP8.5. They used CORDEX data dynamically downscaled from CMIP5 models. In the present study, the same pattern has been obtained for these months during the 2020–2100 period, but with higher values: 2 $m^3s^{-1}km^{-1}year^{-1}$ under SSP2–4.5 and 4 $m^3s^{-1}km^{-1}year^{-1}$ under the SSP5–8.5 scenario. Therefore, it seems that CMIP6 data predict an even higher increase in UI along the western Galician coast throughout the 21st century, compared to CMIP5. Lastly, Sousa et al. (2017) [19] obtained a trend in summer (April to September) upwelling intensity of 1.7 $m^3s^{-1}km^{-1}year^{-1}$, averaging all latitudes covering the WIP for the 2006–2099 period under the CORDEX RCP8.5 scenario. In the present study, the summer UI trend results in a 3.5 $m^3s^{-1}km^{-1}year^{-1}$ for the 2020–2100 period under SSP5–8.5. Additionally, the summer UI trends globally increase when moving northward in latitude, following a similar pattern to that obtained by Sousa et al., (2017) [19], but with trends ranging between 3 and 5 $m^3s^{-1}km^{-1}year^{-1}$ instead of between 0 and 3 $m^3s^{-1}km^{-1}year^{-1}$. Therefore, the use of CMIP6 data indicates a higher UI increase during the 21st century.

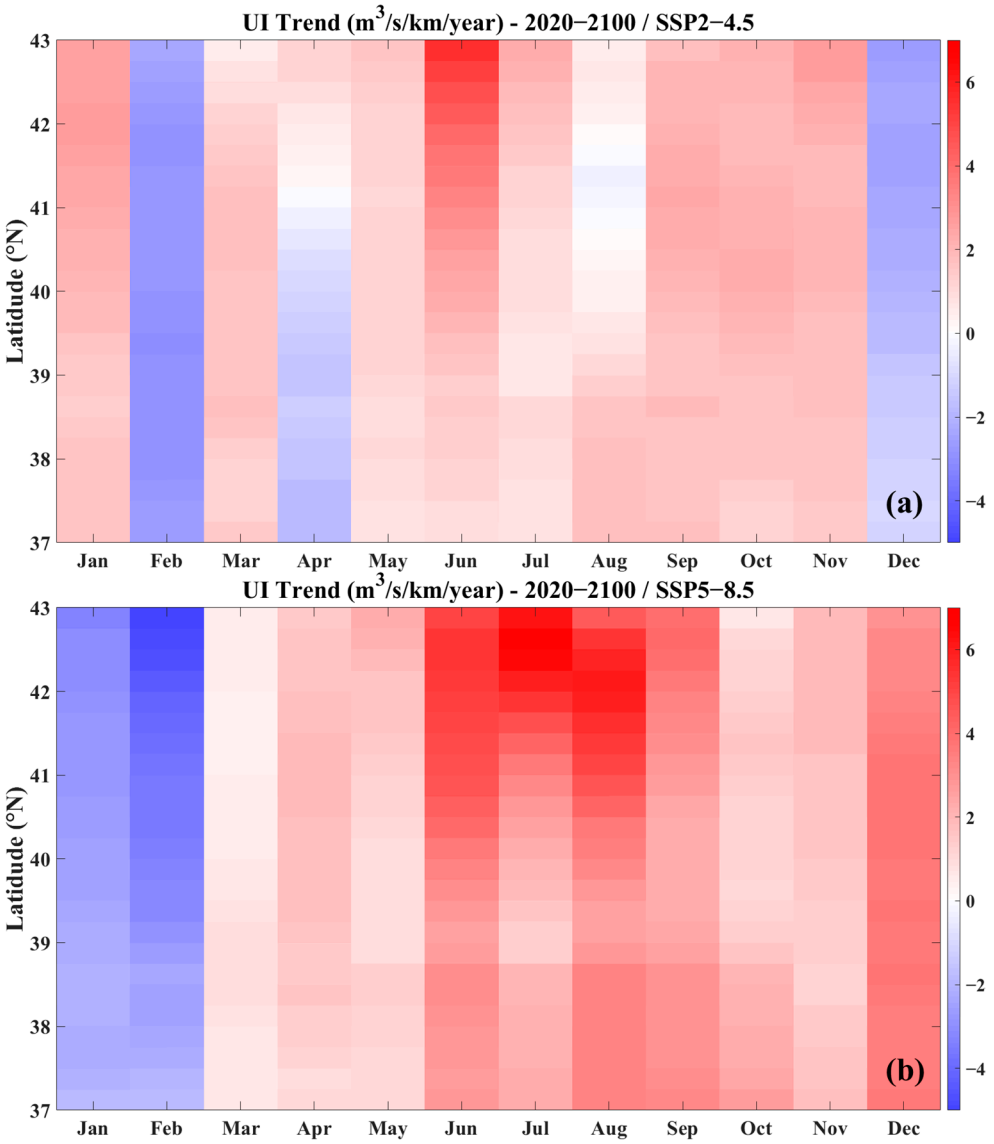


**Figure 6.** UI trends according to the month of the climatic year and the latitude, for the 2020–2100 period under (**a**) SSP2–4.5 and (**b**) SSP5–8.5.

### 3.2.3. Changes during the Upwelling Season

The results previously shown highlight that the months of more intense upwelling conditions range from April to September, whatever the latitude (see Figure 5). Therefore, average UI values over these months have been computed, considering 0.25° latitude intervals, for the historical (1985–2014) and far future (2070–2099) periods. Then, the percentages of difference in UI value between the latter and the former periods were computed in order to study the expected evolution of the upwelling intensity towards the end of the 21st century. Results can be seen in Figure 7 and show that, under SSP2–4.5, the UI will increase a 10% for latitudes southward 39° N and slightly more when moving northward, up to 15% around 43° N. The pattern is the same under the SSP5–8.5 scenario, but with higher UI increments (~20%) between 37° and 39° N and even more northward, reaching more than 35% around 43° N. Consistent with the results obtained in this study, an increase in upwelling during the summer months will be associated with an increase in nutrient availability in the upper layers of the coastal area.

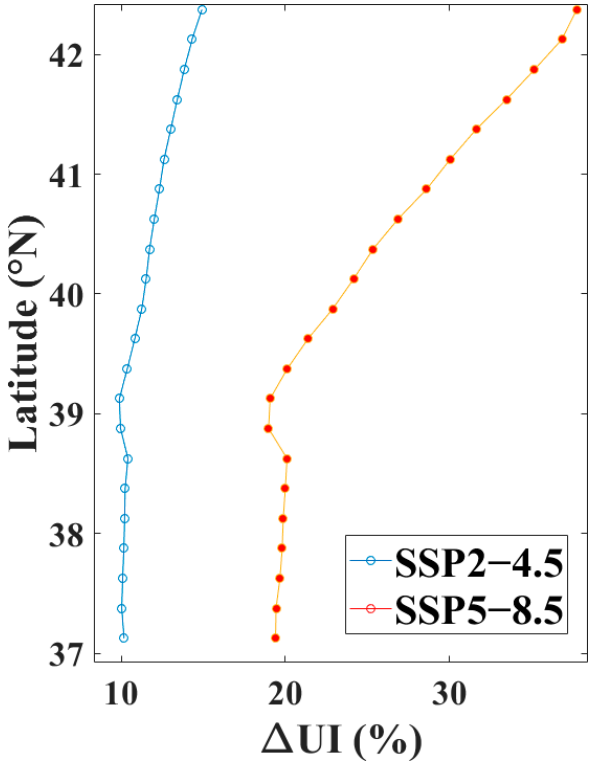


**Figure 7.** ΔUI (%) between the far future (2070–2099) and historical (1985–2014) periods, for the April to September period, according to the latitude and the climate scenario considered. Solid dots correspond to $p < 0.01$ and open circles to $p < 0.05$.

Sousa et al. (2017) [19] computed the average UI along the WIP for the June to September months during the 2080–2099 period under the CORDEX RCP8.5 scenario. They obtained a practically constant UI of around 1100 $m^3s^{-1}km^{-1}$ from 37 to 39.5° N, decreasing up to 500 $m^3s^{-1}km^{-1}$ at 43° N. In the present study, the historical UI between June and September is higher southward (~1050 $m^3s^{-1}km^{-1}$) than northward (~900 $m^3s^{-1}km^{-1}$), as shown in Figure 4. Nevertheless, the ΔUI between historical and far future follow the opposite pattern, especially under SSP5–8.5, as shown in Figure 7. Therefore, when considering CMIP6 data, the summer UI tends to be more homogeneous along the WIP coast in the far future. Actually, it will only range from 1000 to 1250 $m^3s^{-1}km^{-1}$ in the far future under SSP5–8.5, whatever the latitude (Figure 4).

Additionally, the inter-annual evolution of the summer UI (April to September) during the 21st century considering the SSP5–8.5 scenario is shown in Figure A1 from Appendix A.

### *3.3. Spatiotemporal Evolution of the Azores High*

The behavior of the upwelling along the WIP coast is highly determined by the Azores High. The intensity evolution and displacement of the Azores High were analyzed for the 2020–2100 period (Figure 8). April to September SLP values were averaged for the near future (2030–2059) and far future (2070–2099) periods under SSP5–8.5, the climate scenario resulting in the most significant changes in the UI. The results indicate an expected intensification and northward displacement of the Azores High during the 21st century.

April to September SLP values were yearly averaged from 2020 to 2100 to calculate intensity and displacement trends in the Azores High. Results depict an increase in the Azores High's intensity around 0.1 hPa per decade ($p < 0.03$) under SSP5–8.5, as well as its displacement northward close to 0.25° per decade ($p < 0.02$). No significant longitudinal displacement is observed. When considering the SSP2–4.5 climate scenario, no significant pattern is found, neither in position nor intensity changes of the Azores High along the 21st century.

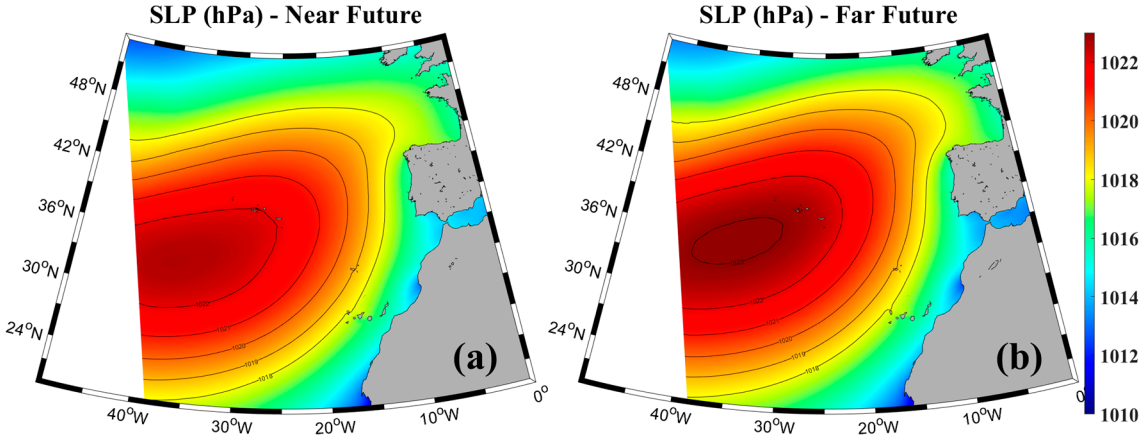


**Figure 8.** Average SLP for the months between April and September for the (**a**) near future (2030–2059) and (**b**) far future (2070–2099), under SSP5–8.5.

Sousa et al. (2017) [19], performing a similar analysis but with coarse-resolution data ranging from 1.12° to 1.8°, found that the Azores High is expected to increase by 0.03 hPa per decade and displace northward around 10 km per decade, for the June to September months during the 2006–2099 period under the CMIP5 RCP8.5 scenario. Therefore, the results found in the present study, using 30 km spatial resolution data, show the same patterns in the Azores High evolution (both in intensity and location), but with magnitudes about 3 times higher. These findings highlight the significant impact of the Azores High's strengthening and shift on upwelling in the northern WIP throughout the 21st century.

## 4. Conclusions

This study aimed to evaluate the changes in upwelling intensity and seasonality in the WIP throughout the 21st century. It involved analyzing both the historical and future climatology of upwelling as well as trends indicating its evolution over time. Additionally, the study examines changes in the position and intensity of the Azores High. Due to the coastal upwelling being a local phenomenon, high spatial resolution data is required. Therefore, data from the latest climate projections—CMIP6—were dynamically downscaled using the WRF model. Wind and SLP data with a 10 km and 30 km spatial resolution, respectively, were obtained in the area under study for a historical period (1985–2014) and the future one (2020–2100) under SSP2–4.5 and SSP5–8.5 representing intermediate and high GHG emissions climate scenarios, respectively. The enhanced spatial resolution of the data permitted us to perform the analysis in the WIP area, representing the northern part of the CUE, where the upwelling is mainly characterized by its seasonality. Once the accuracy of the modeled data is validated, the following key findings can be highlighted:

- Along the WIP coast, the seasonality of the upwelling will not be impacted by climate change. Consequently, the intensity of the monthly UI will continue to reach its highest values from April to September.
- An increase in UI is expected throughout the 21st century during these months of intense upwelling, as well as a decrease for those characterized by weak upwelling.
- Considering the months from April to September, the highest increases in UI are expected at the end of the century and in northern locations of the WIP. Therefore, a homogenization of the UI according to the latitude in the WIP is expected towards the end of the century.
- These changes are a consequence of the expected intensification and northward displacement of the Azores High.

Understanding future trends in coastal upwelling at a finer scale, using dynamically downscaled data, is particularly crucial for the WIP coast, which is noted for its high primary production that supports the fishery industry. This knowledge is vital for optimizing

resources and enhancing fisheries and aquaculture operations. Additionally, a similar study for the remaining areas of the CUE would be of great interest. Two shared socioeconomic pathways have been considered in this study to reduce uncertainties associated with future climate projections. However, it is important to note that some uncertainties remain, such as the potential occurrence of extreme events or rapid changes in components of the climate system, like the Atlantic Meridional Overturning Circulation (AMOC), which would undoubtedly have a significant impact on the study area. Therefore, it will be valuable to conduct a similar analysis in the future when new climate projections become available.

**Author Contributions:** All authors have contributed to the research and writing of this paper. Conceptualization, B.T., X.C., M.d. and M.G.-G.; methodology, B.T., X.C., M.d. and M.G.-G.; software, B.T.; validation, B.T., X.C., M.d. and M.G.-G.; formal analysis, B.T., X.C., M.d. and M.G.-G.; investigation, B.T., X.C., M.d. and M.G.-G.; resources, X.C., M.d. and M.G.-G.; data curation, B.T.; writing—original draft preparation, B.T.; writing—review and editing, X.C., M.d. and M.G.-G.; visualization, B.T.; supervision, X.C., M.d. and M.G.-G.; project administration, X.C., M.d. and M.G.-G.; funding acquisition, X.C., M.d. and M.G.-G. All authors have read and agreed to the published version of the manuscript.

**Funding:** This work was partially supported by Xunta de Galicia under project ED431C 2021/44 (Grupos de Referencia Competitiva) and by MCIN/AEI/10.13039/501100011033 (call under project TED2021-129524B-I00 (RECOBI project). X. Costoya is funded by Grant IJC2020-043745-I (Juan de la Cierva Postdoctoral Fellowship) funded by MCIN/AEI/10.13039/501100011033 and by the "European Union NextGenerationEU/PRTR".

**Institutional Review Board Statement:** Not applicable.

**Informed Consent Statement:** Not applicable.

**Data Availability Statement:** Data will be made available on request.

**Acknowledgments:** Computation took place at Finisterrae III supercomputer that belongs to CESGA (Centro de Supercomputación de Galicia) located at Santiago de Compostela, Galicia.

**Conflicts of Interest:** The authors declare no conflicts of interest.

## Appendix A

**Table A1.** Monthly averaged UI values ($m^3s^{-1}km^{-1}$) for the near future (2030–2059) under SSP2–4.5. The latitude value corresponds to the northern limit of the area, which extends from it to 0.25° southward.

| Lat (°) | January | February | March | April | May | June | July | August | September | October | November | December |
|---|---|---|---|---|---|---|---|---|---|---|---|---|
| 43 | −310 | −8 | 241 | 644 | 626 | 829 | 959 | 887 | 575 | 85 | 16 | −163 |
| 42.75 | −285 | 9 | 253 | 663 | 657 | 887 | 1065 | 966 | 577 | 102 | 26 | −151 |
| 42.5 | −269 | 25 | 254 | 667 | 657 | 891 | 1102 | 989 | 563 | 110 | 36 | −145 |
| 42.25 | −250 | 42 | 264 | 677 | 663 | 894 | 1125 | 1006 | 559 | 122 | 48 | −134 |
| 42 | −220 | 59 | 285 | 689 | 672 | 899 | 1146 | 1031 | 567 | 140 | 69 | −108 |
| 41.75 | −185 | 82 | 304 | 704 | 681 | 903 | 1159 | 1054 | 582 | 156 | 94 | −83 |
| 41.5 | −152 | 108 | 324 | 717 | 693 | 906 | 1169 | 1068 | 593 | 171 | 120 | −62 |
| 41.25 | −131 | 130 | 340 | 727 | 702 | 903 | 1168 | 1064 | 599 | 184 | 136 | −52 |
| 41 | −111 | 148 | 354 | 734 | 706 | 895 | 1160 | 1053 | 602 | 192 | 147 | −40 |
| 40.75 | −92 | 166 | 367 | 734 | 704 | 885 | 1139 | 1031 | 599 | 195 | 153 | −30 |
| 40.5 | −73 | 184 | 379 | 734 | 702 | 876 | 1115 | 1003 | 592 | 200 | 156 | −20 |
| 40.25 | −54 | 197 | 388 | 734 | 699 | 866 | 1093 | 981 | 586 | 203 | 163 | −9 |
| 40 | −31 | 209 | 399 | 731 | 697 | 856 | 1074 | 961 | 582 | 208 | 174 | 2 |
| 39.75 | −8 | 224 | 413 | 728 | 699 | 849 | 1057 | 939 | 579 | 218 | 188 | 16 |
| 39.5 | 20 | 244 | 429 | 727 | 707 | 856 | 1056 | 931 | 580 | 231 | 204 | 36 |
| 39.25 | 53 | 266 | 450 | 737 | 723 | 879 | 1075 | 941 | 593 | 252 | 224 | 65 |
| 39 | 75 | 281 | 465 | 750 | 753 | 924 | 1128 | 982 | 621 | 277 | 235 | 80 |
| 38.75 | 111 | 321 | 510 | 798 | 842 | 1046 | 1277 | 1117 | 705 | 330 | 262 | 107 |
| 38.5 | 136 | 340 | 527 | 803 | 844 | 1046 | 1273 | 1113 | 720 | 347 | 285 | 134 |
| 38.25 | 138 | 335 | 516 | 775 | 812 | 1010 | 1239 | 1078 | 701 | 336 | 285 | 132 |
| 38 | 138 | 330 | 504 | 753 | 791 | 988 | 1221 | 1056 | 682 | 326 | 280 | 127 |
| 37.75 | 140 | 325 | 486 | 734 | 778 | 972 | 1210 | 1044 | 669 | 318 | 273 | 121 |
| 37.5 | 145 | 324 | 467 | 714 | 769 | 961 | 1209 | 1041 | 657 | 312 | 267 | 117 |
| 37.25 | 160 | 336 | 469 | 706 | 775 | 966 | 1222 | 1050 | 655 | 318 | 277 | 133 |

**Table A2.** Monthly averaged UI values ($m^3s^{-1}km^{-1}$) for the near future (2030–2059) under SSP5–8.5. The latitude value corresponds to the northern limit of the area, which extends from it to 0.25° southward.

| Lat (°) | January | February | March | April | May | June | July | August | September | October | November | December |
|---|---|---|---|---|---|---|---|---|---|---|---|---|
| 43 | −92 | 98 | 201 | 653 | 761 | 924 | 1064 | 863 | 572 | 144 | 64 | −242 |
| 42.75 | −78 | 103 | 218 | 671 | 800 | 977 | 1164 | 936 | 581 | 161 | 74 | −232 |
| 42.5 | −64 | 110 | 224 | 669 | 801 | 969 | 1194 | 957 | 566 | 165 | 83 | −225 |
| 42.25 | −45 | 122 | 242 | 672 | 805 | 962 | 1214 | 976 | 562 | 176 | 97 | −215 |
| 42 | −21 | 141 | 269 | 683 | 810 | 961 | 1240 | 1001 | 571 | 193 | 120 | −196 |
| 41.75 | 8 | 158 | 295 | 696 | 814 | 959 | 1258 | 1024 | 583 | 212 | 140 | −174 |
| 41.5 | 43 | 171 | 315 | 705 | 820 | 956 | 1267 | 1037 | 591 | 229 | 161 | −153 |
| 41.25 | 70 | 180 | 329 | 712 | 821 | 949 | 1264 | 1039 | 597 | 244 | 176 | −140 |
| 41 | 89 | 186 | 338 | 717 | 817 | 938 | 1254 | 1032 | 595 | 256 | 185 | −125 |
| 40.75 | 105 | 191 | 349 | 714 | 802 | 921 | 1234 | 1017 | 589 | 264 | 191 | −109 |
| 40.5 | 121 | 200 | 358 | 710 | 789 | 902 | 1209 | 997 | 583 | 270 | 200 | −93 |
| 40.25 | 138 | 213 | 367 | 708 | 778 | 888 | 1185 | 978 | 580 | 277 | 210 | −75 |
| 40 | 153 | 224 | 375 | 706 | 765 | 873 | 1164 | 961 | 578 | 286 | 221 | −56 |
| 39.75 | 169 | 237 | 383 | 706 | 755 | 860 | 1142 | 945 | 576 | 297 | 230 | −36 |
| 39.5 | 187 | 251 | 396 | 715 | 754 | 860 | 1136 | 944 | 582 | 310 | 242 | −12 |
| 39.25 | 215 | 269 | 409 | 728 | 768 | 876 | 1150 | 956 | 601 | 330 | 261 | 21 |
| 39 | 230 | 279 | 430 | 752 | 798 | 913 | 1203 | 1002 | 631 | 351 | 272 | 32 |
| 38.75 | 255 | 306 | 479 | 813 | 887 | 1036 | 1365 | 1142 | 715 | 397 | 297 | 56 |
| 38.5 | 282 | 331 | 493 | 816 | 884 | 1035 | 1358 | 1146 | 722 | 413 | 317 | 93 |
| 38.25 | 288 | 329 | 481 | 794 | 850 | 1001 | 1316 | 1114 | 700 | 405 | 315 | 101 |
| 38 | 290 | 321 | 470 | 772 | 827 | 980 | 1294 | 1096 | 685 | 397 | 309 | 101 |
| 37.75 | 287 | 305 | 459 | 754 | 809 | 960 | 1280 | 1087 | 675 | 388 | 304 | 101 |
| 37.5 | 285 | 290 | 454 | 736 | 791 | 949 | 1275 | 1086 | 666 | 378 | 301 | 106 |
| 37.25 | 289 | 295 | 460 | 727 | 787 | 953 | 1282 | 1101 | 672 | 382 | 316 | 117 |

**Table A3.** Monthly averaged UI values ($m^3s^{-1}km^{-1}$) for the far future (2070–2099) under SSP2–4.5. The latitude value corresponds to the northern limit of the area, which extends from it to 0.25° southward.

| Lat (°) | January | February | March | April | May | June | July | August | September | October | November | December |
|---|---|---|---|---|---|---|---|---|---|---|---|---|
| 43 | −204 | −17 | 259 | 629 | 685 | 998 | 1041 | 871 | 623 | 83 | 155 | −280 |
| 42.75 | −186 | −11 | 283 | 649 | 709 | 1039 | 1142 | 942 | 635 | 104 | 154 | −258 |
| 42.5 | −174 | −6 | 294 | 646 | 703 | 1028 | 1168 | 956 | 613 | 116 | 149 | −245 |
| 42.25 | −155 | 2 | 313 | 650 | 703 | 1019 | 1183 | 966 | 601 | 131 | 152 | −233 |
| 42 | −128 | 16 | 340 | 664 | 714 | 1014 | 1196 | 984 | 604 | 152 | 158 | −208 |
| 41.75 | −100 | 41 | 363 | 678 | 728 | 1014 | 1203 | 1000 | 611 | 172 | 166 | −179 |
| 41.5 | −71 | 64 | 385 | 690 | 740 | 1013 | 1203 | 1011 | 619 | 190 | 180 | −150 |
| 41.25 | −51 | 83 | 401 | 694 | 748 | 1008 | 1196 | 1014 | 620 | 206 | 196 | −128 |
| 41 | −37 | 98 | 411 | 692 | 751 | 997 | 1182 | 1012 | 618 | 217 | 208 | −110 |
| 40.75 | −22 | 111 | 418 | 686 | 750 | 980 | 1157 | 1003 | 609 | 226 | 212 | −90 |
| 40.5 | −7 | 118 | 425 | 680 | 746 | 961 | 1130 | 988 | 596 | 235 | 217 | −71 |
| 40.25 | 6 | 127 | 429 | 675 | 743 | 946 | 1108 | 975 | 587 | 239 | 222 | −52 |
| 40 | 23 | 136 | 439 | 671 | 742 | 932 | 1087 | 960 | 584 | 243 | 229 | −31 |
| 39.75 | 43 | 147 | 450 | 667 | 744 | 919 | 1064 | 949 | 579 | 247 | 237 | −9 |
| 39.5 | 64 | 161 | 465 | 666 | 752 | 917 | 1059 | 952 | 580 | 257 | 248 | 17 |
| 39.25 | 92 | 182 | 482 | 674 | 768 | 931 | 1073 | 973 | 590 | 274 | 268 | 52 |
| 39 | 108 | 199 | 496 | 693 | 800 | 973 | 1125 | 1026 | 620 | 291 | 279 | 70 |
| 38.75 | 142 | 236 | 538 | 757 | 883 | 1103 | 1290 | 1167 | 709 | 339 | 308 | 99 |
| 38.5 | 172 | 252 | 541 | 757 | 885 | 1100 | 1291 | 1169 | 708 | 356 | 332 | 125 |
| 38.25 | 182 | 245 | 520 | 729 | 859 | 1065 | 1248 | 1140 | 683 | 345 | 330 | 128 |
| 38 | 185 | 236 | 500 | 706 | 842 | 1042 | 1223 | 1125 | 669 | 335 | 325 | 127 |
| 37.75 | 186 | 228 | 477 | 687 | 827 | 1025 | 1210 | 1117 | 659 | 325 | 315 | 127 |
| 37.5 | 187 | 225 | 458 | 670 | 816 | 1014 | 1203 | 1117 | 652 | 318 | 309 | 132 |
| 37.25 | 196 | 235 | 468 | 668 | 820 | 1016 | 1216 | 1128 | 660 | 328 | 317 | 142 |

**Table A4.** Monthly averaged UI values ($m^3s^{-1}km^{-1}$) for the far future (2070–2099) under SSP5–8.5. The latitude value corresponds to the northern limit of the area, which extends from it to 0.25° southward.

| Lat (°) | January | February | March | April | May | June | July | August | September | October | November | December |
|---|---|---|---|---|---|---|---|---|---|---|---|---|
| 43 | −333 | −248 | 251 | 664 | 811 | 1125 | 1290 | 1064 | 793 | 102 | 106 | −134 |
| 42.75 | −310 | −221 | 255 | 682 | 849 | 1195 | 1402 | 1188 | 800 | 122 | 115 | −112 |
| 42.5 | −297 | −203 | 249 | 681 | 843 | 1188 | 1415 | 1234 | 771 | 127 | 120 | −98 |
| 42.25 | −282 | −180 | 253 | 693 | 840 | 1175 | 1409 | 1262 | 753 | 140 | 127 | −81 |
| 42 | −254 | −144 | 267 | 710 | 846 | 1163 | 1398 | 1286 | 743 | 159 | 139 | −55 |
| 41.75 | −221 | −112 | 288 | 728 | 854 | 1154 | 1384 | 1298 | 742 | 180 | 160 | −21 |
| 41.5 | −190 | −84 | 311 | 744 | 859 | 1141 | 1365 | 1298 | 736 | 202 | 180 | 9 |
| 41.25 | −168 | −63 | 331 | 756 | 861 | 1124 | 1343 | 1288 | 727 | 219 | 192 | 33 |
| 41 | −153 | −47 | 344 | 763 | 857 | 1098 | 1312 | 1269 | 714 | 228 | 199 | 48 |
| 40.75 | −135 | −32 | 353 | 760 | 848 | 1061 | 1271 | 1237 | 694 | 233 | 205 | 62 |
| 40.5 | −117 | −15 | 362 | 755 | 836 | 1026 | 1232 | 1201 | 674 | 240 | 210 | 74 |
| 40.25 | −100 | 3 | 370 | 751 | 825 | 996 | 1200 | 1170 | 662 | 247 | 218 | 86 |
| 40 | −83 | 22 | 383 | 750 | 817 | 967 | 1169 | 1139 | 654 | 256 | 229 | 99 |
| 39.75 | −66 | 44 | 398 | 747 | 810 | 941 | 1140 | 1106 | 648 | 269 | 237 | 115 |
| 39.5 | −42 | 67 | 417 | 751 | 815 | 928 | 1128 | 1090 | 649 | 286 | 252 | 138 |
| 39.25 | −12 | 100 | 441 | 762 | 834 | 933 | 1134 | 1100 | 664 | 316 | 272 | 161 |
| 39 | 6 | 124 | 461 | 779 | 867 | 974 | 1190 | 1156 | 699 | 348 | 285 | 180 |
| 38.75 | 38 | 169 | 510 | 848 | 972 | 1115 | 1372 | 1323 | 797 | 415 | 313 | 216 |
| 38.5 | 64 | 192 | 528 | 858 | 973 | 1111 | 1368 | 1324 | 798 | 438 | 335 | 244 |
| 38.25 | 63 | 191 | 513 | 824 | 936 | 1068 | 1333 | 1290 | 775 | 435 | 338 | 245 |
| 38 | 61 | 185 | 499 | 801 | 911 | 1040 | 1316 | 1271 | 758 | 430 | 334 | 244 |
| 37.75 | 60 | 178 | 484 | 778 | 895 | 1019 | 1309 | 1261 | 745 | 427 | 326 | 246 |
| 37.5 | 64 | 177 | 472 | 755 | 881 | 1004 | 1307 | 1257 | 737 | 426 | 323 | 251 |
| 37.25 | 85 | 191 | 481 | 753 | 879 | 1007 | 1318 | 1267 | 745 | 438 | 337 | 265 |

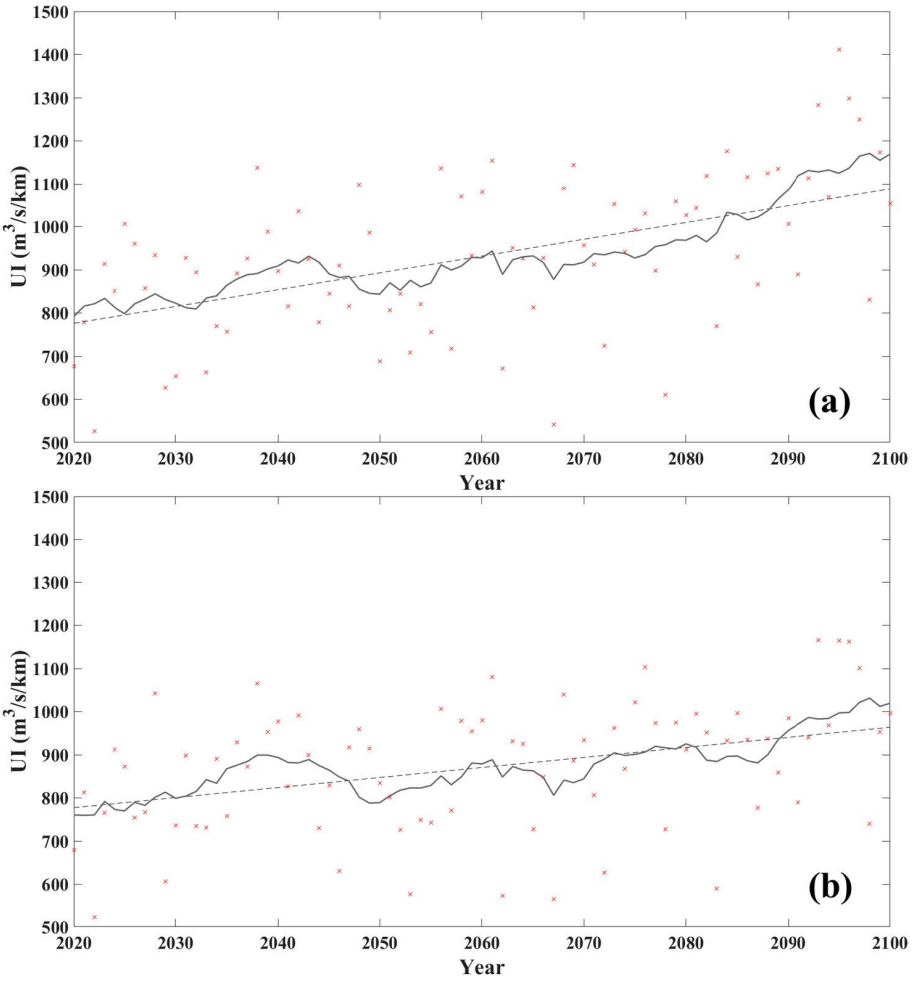


**Figure A1.** *Cont.*

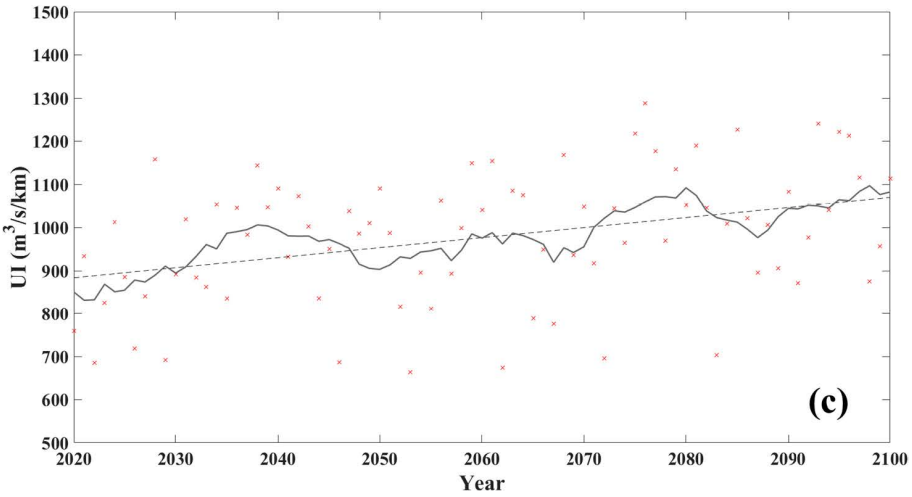


**Figure A1.** Annual evolution of the summer UI during the 21st century under SSP5–8.5 for 1°-latitude ranges centered at (**a**) 42°, (**b**) 40°, and (**c**) 38°. Red crosses represent the raw values, the dotted line indicates the linear trend, and the solid line represents the 10-year moving average.

## References


1. Pauly, D.; Christensen, V. Primary production required to sustain global fisheries. *Nature* **1995**, *374*, 255–257. [CrossRef]
2. Arístegui, J.; Barton, E.D.; Álvarez-Salgado, X.A.; Santos, A.M.P.; Figueiras, F.G.; Kifani, S.; Hernández-León, S.; Mason, E.; Machú, E.; Demarcq, H. Sub-regional ecosystem variability in the Canary Current upwelling. *Prog. Oceanogr.* **2009**, *83*, 33–48. [CrossRef]
3. Cropper, T.E.; Hanna, E.; Bigg, G.R. Spatial and temporal seasonal trends in coastal upwelling off Northwest Africa, 1981–2012. *Deep Sea Res. Part I Oceanogr. Res. Pap.* **2014**, *86*, 94–111. [CrossRef]
4. Gómez-Letona, M.; Ramos, A.G.; Coca, J.; Arístegui, J. Trends in primary production in the canary current upwelling system—A regional perspective comparing remote sensing models. *Front. Mar. Sci.* **2017**, *4*, 370. [CrossRef]
5. Bakun, A. Global climate change and intensification of coastal ocean upwelling. *Science* **1990**, *247*, 198–201. [CrossRef]
6. Bakun, A.; Field, D.B.; Redondo-Rodriguez, A.; Weeks, S.J. Greenhouse gas, upwelling-favorable winds, and the future of coastal ocean upwelling ecosystems. *Glob. Chang. Biol.* **2010**, *16*, 1213–1228. [CrossRef]
7. Narayan, N.; Paul, A.; Mulitza, S.; Schulz, M. Trends in coastal upwelling intensity during the late 20th century. *Ocean Sci.* **2010**, *6*, 815–823. [CrossRef]
8. Gutiérrez, D.; Bouloubassi, I.; Sifeddine, A.; Purca, S.; Goubanova, K.; Graco, M.; Field, D.; Méjanelle, L.; Velazco, F.; Lorre, A.; et al. Coastal cooling and increased productivity in the main upwelling zone off Peru since the mid-twentieth century. *Geophys. Res. Lett.* **2011**, *38*, 7. [CrossRef]
9. Barton, E.; Field, D.; Roy, C. Canary current upwelling: More or less? *Prog. Oceanogr.* **2013**, *116*, 167–178. [CrossRef]
10. Bakun, A.; Black, B.A.; Bograd, S.J.; García-Reyes, M.; Miller, A.J.; Rykaczewski, R.R.; Sydeman, W.J. Anticipated effects of climate change on coastal upwelling ecosystems. *Curr. Clim. Chang. Rep.* **2015**, *1*, 85–93. [CrossRef]
11. Sydeman, W.J.; García-Reyes, M.; Schoeman, D.S.; Rykaczewski, R.R.; Thompson, S.A.; Black, B.A.; Bograd, S.J. Climate change and wind intensification in coastal upwelling ecosystems. *Science* **2014**, *345*, 77–80. [CrossRef] [PubMed]
12. Varela, R.; Álvarez, I.; Santos, F.; Decastro, M.; Gómez-Gesteira, M. Has upwelling strengthened along worldwide coasts over 1982–2010? *Sci. Rep.* **2015**, *5*, 10016. [CrossRef] [PubMed]
13. Eyring, V.; Bony, S.; Meehl, G.A.; Senior, C.A.; Stevens, B.; Stouffer, R.J.; Taylor, K.E. Overview of the Coupled Model Intercomparison Project Phase 6 (CMIP6) experimental design and organization. *Geosci. Model Dev.* **2016**, *9*, 1937–1958. [CrossRef]
14. Riahi, K.; Van Vuuren, D.P.; Kriegler, E.; Edmonds, J.; O'Neill, B.C.; Fujimori, S.; Bauer, N.; Calvin, K.; Dellink, R.; Fricko, O.; et al. The Shared Socioeconomic Pathways and their energy, land use, and greenhouse gas emissions implications: An overview. *Glob. Environ. Chang.* **2017**, *42*, 153–168. [CrossRef]
15. Moss, R.H.; Edmonds, J.A.; Hibbard, K.A.; Manning, M.R.; Rose, S.K.; Van Vuuren, D.P.; Carter, T.R.; Emori, S.; Kainuma, M.; Kram, T. The next generation of scenarios for climate change research and assessment. *Nature* **2010**, *463*, 747–756. [CrossRef] [PubMed]
16. Rykaczewski, R.R.; Dunne, J.P.; Sydeman, W.J.; García-Reyes, M.; Black, B.A.; Bograd, S.J. Poleward displacement of coastal upwelling-favorable winds in the ocean's eastern boundary currents through the 21st century. *Geophys. Res. Lett.* **2015**, *42*, 6424–6431. [CrossRef]
17. Bograd, S.J.; Jacox, M.G.; Hazen, E.L.; Lovecchio, E.; Montes, I.; Buil, M.P.; Shannon, L.J.; Sydeman, W.J.; Rykaczewski, R.R. Climate change impacts on eastern boundary upwelling systems. *Annu. Rev. Mar. Sci.* **2023**, *15*, 303–328. [CrossRef]
18. Alvarez, I.; Lorenzo, M.N.; Decastro, M.; Gomez-Gesteira, M. Coastal upwelling trends under future warming scenarios from the CORDEX project along the Galician coast (NW Iberian Peninsula). *Int. J. Clim.* **2016**, *37*, 3427–3438. [CrossRef]

19. Sousa, M.C.; Decastro, M.; Alvarez, I.; Gomez-Gesteira, M.; Dias, J.M. Why coastal upwelling is expected to increase along the western Iberian Peninsula over the next century? *Sci. Total Environ.* **2017**, *592*, 243–251. [CrossRef]
20. Vázquez, R.; Parras-Berrocal, I.; Koseki, S.; Cabos, W.; Sein, D.; Izquierdo, A. Seasonality of Coastal Upwelling Trends in the Mauritania-Senegalese Region under RCP8.5 Climate Change Scenario. *Sci. Total Environ.* **2023**, *898*, 166391. [CrossRef]
21. Vázquez, R.; Parras-Berrocal, I.M.; Cabos, W.; Sein, D.; Mañanes, R.; Bolado-Penagos, M.; Izquierdo, A. Climate Change in the Canary/Iberia Upwelling Region: The Role of Ocean Stratification and Wind. *Environ. Res. Lett.* **2024**, *19*, 074064. [CrossRef]
22. Skamarock, W.C.; Klemp, J.B.; Dudhia, J.; Gill, D.O.; Zhiquan, L.; Berner, J.; Wang, W.; Powers, J.G.; Duda, M.G.; Barker, D.M.; et al. *A Description of the Advanced Research WRF Model Version 4.3*; No. NCAR/TN-556+STR; National Center for Atmospheric Research: Boulder, CO, USA, 2021. [CrossRef]
23. Xu, Z.; Han, Y.; Tam, C.-Y.; Yang, Z.-L.; Fu, C. Bias-corrected CMIP6 global dataset for dynamical downscaling of the historical and future climate (1979–2100). *Sci. Data* **2021**, *8*, 293. [CrossRef]
24. Hersbach, H.; Bell, B.; Berrisford, P.; Hirahara, S.; Horányi, A.; Muñoz-Sabater, J.; Nicolas, J.; Peubey, C.; Radu, R.; Schepers, D.; et al. The ERA5 global reanalysis. *Q. J. R. Meteorol. Soc.* **2020**, *146*, 1999–2049. [CrossRef]
25. Horvath, K.; Koracin, D.; Vellore, R.; Jiang, J.; Belu, R. Sub-kilometer dynamical downscaling of near-surface winds in complex terrain using WRF and MM5 mesoscale models. *J. Geophys. Res. Atmos.* **2012**, *117*, D11. [CrossRef]
26. Jerez, S.; López-Romero, J.M.; Turco, M.; Lorente-Plazas, R.; Gómez-Navarro, J.J.; Jiménez-Guerrero, P.; Montávez, J.P. On the spin-up period in WRF simulations over europe: Trade-offs between length and seasonality. *J. Adv. Model. Earth Syst.* **2020**, *12*, 4. [CrossRef]
27. Lo, J.C.; Yang, Z.; Pielke, R.A. Assessment of three dynamical climate downscaling methods using the Weather Research and Forecasting (WRF) model. *J. Geophys. Res. Atmos.* **2008**, *113*, D9. [CrossRef]
28. Pan, Z.; Takle, E.; Gutowski, W.; Turner, R. Long simulation of regional climate as a sequence of short segments. *Mon. Weather. Rev.* **1999**, *127*, 308–321. [CrossRef]
29. Qian, J.-H.; Seth, A.; Zebiak, S. Reinitialized versus continuous simulations for regional climate downscaling. *Mon. Weather. Rev.* **2003**, *131*, 2857–2874. [CrossRef]
30. Thomas, B.; Costoya, X.; Decastro, M.; Insua-Costa, D.; Senande-Rivera, M.; Gómez-Gesteira, M. Downscaling CMIP6 climate projections to classify the future offshore wind energy resource in the Spanish territorial waters. *J. Clean. Prod.* **2023**, *433*, 139860. [CrossRef]
31. Thompson, G.; Field, P.R.; Rasmussen, R.M.; Hall, W.D. Explicit forecasts of winter precipitation using an improved bulk microphysics scheme. Part II: Implementation of a new snow parameterization. *Mon. Weather Rev.* **2008**, *136*, 5095–5115. [CrossRef]
32. Hong, S.-Y.; Noh, Y.; Dudhia, J. A new vertical diffusion package with an explicit treatment of entrainment processes. *Mon. Weather. Rev.* **2006**, *134*, 2318–2341. [CrossRef]
33. Tewari, M.; Chen, F.; Wang, W.; Dudhia, J.; LeMone, M.A.; Mitchell, K.; Ek, M.; Gayno, G.; Wegiel, J.; Cuenca, R.H. Implementation and Verification of the Unified Noah Land Surface Model in the WRF Model. In Proceedings of the 20th Conference on Weather Analysis and Forecasting/16th Conference on Numerical Weather Prediction, Seattle, WA, USA, 2004; American Meteorological Society, 14.2a. Available online: https://ams.confex.com/ams/84Annual/techprogram/paper_69061.htm (accessed on 22 July 2024).
34. Jiménez, P.A.; Dudhia, J.; González-Rouco, J.F.; Navarro, J.; Montávez, J.P.; García-Bustamante, E. A revised scheme for the WRF surface layer formulation. *Mon. Weather. Rev.* **2012**, *140*, 898–918. [CrossRef]
35. Iacono, M.J.; Delamere, J.S.; Mlawer, E.J.; Shephard, M.W.; Clough, S.A.; Collins, W.D. Radiative forcing by long-lived greenhouse gases: Calculations with the AER radiative transfer models. *J. Geophys. Res. Atmos.* **2008**, *113*, D13103. [CrossRef]
36. Zhang, C.; Wang, Y. Projected future changes of tropical cyclone activity over the Western North and South Pacific in a 20-km-mesh regional climate model. *J. Clim.* **2017**, *30*, 5923–5941. [CrossRef]
37. Perkins, S.E.; Pitman, A.J.; Holbrook, N.J.; McAneney, J. Evaluation of the AR4 climate models' simulated daily maximum temperature, minimum temperature, and precipitation over Australia using probability density functions. *J. Clim.* **2007**, *20*, 4356–4376. [CrossRef]
38. Press, W.H.; Teukolsky, S.A.; Vetterling, W.T.; Flannery, B.P. *Numerical Recipes in C*, 2nd ed.; Cambridge University Press: Cambridge, UK, 1992.
39. Beaucage, P.; Glazer, A.; Choisnard, J.; Yu, W.; Bernier, M.; Benoit, R.; Lafrance, G. Wind Assessment in a Coastal Environment Using Synthetic Aperture Radar Satellite Imagery and a Numerical Weather Prediction Model. *Can. J. Remote Sens.* **2007**, *33*, 368–377. [CrossRef]
40. Picado, A.; Lorenzo, M.N.; Alvarez, I.; Decastro, M.; Vaz, N.; Dias, J.M. Upwelling and Chl-a spatiotemporal variability along the Galician coast: Dependence on circulation weather types. *Int. J. Clim.* **2015**, *36*, 3280–3296. [CrossRef]
41. Decastro, M.; Gómez-Gesteira, M.; Costoya, X.; Santos, F. Upwelling influence on the number of extreme hot SST days along the Canary upwelling ecosystem. *J. Geophys. Res. Oceans* **2014**, *119*, 3029–3040. [CrossRef]